Article

Strong Pyro-Electro-Chemical Coupling of Elbaite/H$_2$O$_2$ System for Pyrocatalysis Dye Wastewater

Fei Chen [1], Jiesen Guo [1], Dezhong Meng [1,2,*], Yuetong Wu [1], Ruijin Sun [1] and Changchun Zhao [1,*]

[1] School of Science, China University of Geosciences (Beijing), Beijing 100083, China; cf15612189105@163.com (F.C.); Jason950616@163.com (J.G.); wuyuetong2020@outlook.com (Y.W.); sunruijin@cugb.edu.cn (R.S.)

[2] Zhengzhou Institute, China University of Geosciences (Beijing), Zhengzhou 451283, China

* Correspondence: meng@cugb.edu.cn (D.M.); 2011010020@cugb.edu.cn (C.Z.); Tel.: +86-10-8232-1062 (D.M.); +86-10-8232-3426 (C.Z.)

Abstract: Elbaite is a natural silicate mineral with a spontaneous electric field. In the current study, it was selected as a pyroelectric catalyst to promote hydrogen peroxide (H$_2$O$_2$) for dye decomposition due to its pyro-electro-chemical coupling. The behaviors and efficiency of the elbaite/H$_2$O$_2$ system in rhodamine B (RhB) degradation were systematically investigated. The results indicate that the optimal effective degradability of RhB reaches 100.0% at 4.0 g/L elbaite, 7.0 mL/L H$_2$O$_2$, and pH = 2.0 in the elbaite/H$_2$O$_2$ system. The elbaite/H$_2$O$_2$ system exhibits high recyclability and stability after recycling three times, reaching 94.5% of the degradation rate. The mechanisms of RhB degradation clarified that the hydroxyl radical (·OH) is the main active specie involved in catalytic degradation in the elbaite/H$_2$O$_2$ system. Moreover, not only does elbaite act as a pyroelectric catalyst to activate H$_2$O$_2$ in order to generate the primary ·OH for subsequent advanced oxidation reactions, but it also has the role of a dye sorbent. The elbaite/H$_2$O$_2$ system shows excellent application potential for the degradation of RhB.

Keywords: tourmaline; elbaite/H$_2$O$_2$ system; pyroelectric catalyst; dye wastewater; RhB degradation

1. Introduction

The development of synthetic dyes has displayed notable progression since the late 19th century [1]. Dyes without proper treatment are the main source of water pollution, which contains large amounts of polyphenylene ring substituents, showing biotoxicity and chromaticity [2–4]. Moreover, polluted water is gradually developing a resistance to photolysis, antioxidants, and biology [5,6]. Hence, it is an urgent problem for scientists to improve the removal technology of these harmful dyes from wastewater [4]. In order to solve this problem, traditional and modern techniques are raised as common methods to treat dye wastewater. These technologies mainly include coagulation [7], air stripping [8], incineration [9,10], filtration through a membrane [11], adsorption on stimulated carbon [12], electrochemical oxidation [13], wet oxidation [14], biological oxidation [15], and chemical oxidation techniques [16,17]. Among these technologies, chemical oxidation techniques are the most widely used due to the degradation of dye molecules. As one kind of chemical oxidation technique, advanced oxidation process (AOPs) has drawn an increasing amount of attention in the degradation of dyes, specifically, photocatalytic degradation [18–23], Fenton oxidation [24], Fenton-like oxidation [25], and activation of persulfate/peroxymonosulfate (PS/PMS) [26,27]. The reactive species in AOPs are usually the hydroxyl radical (·OH) [28] and hydrated electron (eaq−) [29]. However, there might still be some problems with the application of these technologies. For instance, the possibility of releasing residual-free radical oxidants such as ·OH and producing toxic degradation products [28]. Therefore, it is necessary to develop an efficient and environmentally friendly catalytic treatment technology for dye wastewater. It is well accepted that pyroelectric

materials can generate polarized charges under external thermal excitation. Furthermore, the polarized charge can promote the emergence of powerful oxidant active substances such as ·OH. As a result, heat energy and electrical energy can be used for the degradation of dye wastewater due to the pyro-electric-chemical coupling effect [30,31]. To date, pyroelectric material, $Ba_{0.7}Sr_{0.3}TiO_3$@Ag nanoparticles [32], $NaNbO_3$ nanoparticles [33], $BaTiO_3$ nanofibers [34], ZnO nanorods [35], and Pb $(Zr_{0.52}Ti_{0.48})O_3$ polarized ceramic [36] were found to be effective for the degradation of dyes. Tourmaline is one of the typical natural pyroelectric materials [37]. There are currently several studies on the degradation of dyes by tourmaline [38–42]. Schorl, as an iron-rich tourmaline, can be used as an effective catalyst to enhance the efficiency of reactive free radicals and has been shown to assist in the removal of many organic pollutants, such as fosfomycin and tetracycline in schorl/H_2O_2 systems [39,40]. The heterogeneous Fenton reaction formed by the schorl/H_2O_2 system mainly uses the presence of iron in schorl, but the iron content in schorl is generally not higher than 10%, which has certain limitations in practical application [41,42]. Furthermore, it is reported that tourmaline can be regarded as an excellent adsorbent candidate [38]. The adsorption of tourmaline results from the diffusion of dye molecules into the pores of tourmaline. Although drawbacks remain, it is considered that not only can tourmaline be regarded as a candidate for physical adsorption, but it also has the potential as a catalyst for advanced oxidation technologies.

Elbaite is a typical representative of the tourmaline family. Meanwhile, it is also one of the most promising pyroelectric materials, and its high pyroelectric coefficient can be up to 0.46 nC/cm^2/K [43]. In this study, a new method was proposed in which elbaite was selected to catalyze H_2O_2 for the decomposition of rhodamine B (RhB). The pyro-electro-chemical coupling effect is found in the elbaite/H_2O_2 system, and the decomposition mechanism is well understood. The elbaite/H_2O_2 system has proved to be a potential candidate to deal with dyes.

2. Results and Discussion

2.1. Characterization of Elbaite

The XRD patterns of elbaite are shown in Figure 1a. In these patterns, all reflection peaks can be indexed to previous studies (JCPDS card number PDF#71–716, space group: R3m). No characteristic peaks of other impurities are detected in the pattern. Figure 1b demonstrates the morphology of elbaite with micron-sized particles, generally less than 10 µm. In addition, the EDX spectrums in Figure 1c,d demonstrate the existence of O, Si, Al, Na, F, Ca, and C elements in the sample. Here, C comes from the sample carrier during the SEM sample preparation process. Furthermore, based on the analysis of chemical composition in Table 1, the elbaite applied to this study mainly contains the elements O, Si, Al, S, Mn, Ca, K, Lu, Li, Pb, and Fe, which are virtually consistent with the chemical composition of Figure 1c,d. Since the content of Fe in elbaite is very rare, the effect of the Fenton reaction between elbaite and H_2O_2 can be excluded.

Table 1. Chemical composition analyses of elbaite.

Component	SiO_2	Al_2O_3	SO_3	MnO	CaO	K_2O	Lu_2O_3	Li	PbO	Fe	Total
wt%	51.80	40.50	3.16	1.83	1.68	0.31	0.25	0.23	0.10	0.07	99.93

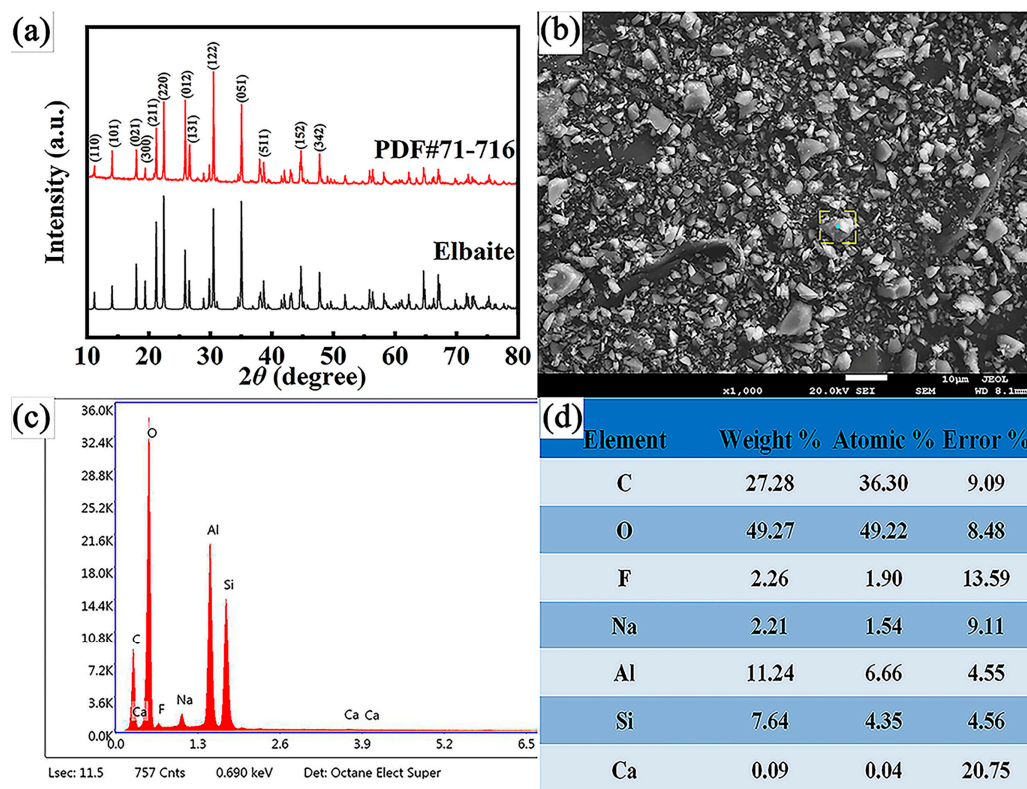Note: Li and Fe elements are detected by ICP-MS. Other elements are detected by XRF and expressed in oxide.

Figure 1. Characterization of elbaite: (**a**) the XRD pattern; (**b**) the SEM image; (**c**) the EDX analysis; and (**d**) the elements content.

2.2. Degradation Factors for Contaminant RhB

The elbaite's pyroelectrically driven activity is determined based on the decomposition of RhB dye. Figure 2a shows the change in concentration of RhB solution without any catalyst under acidic conditions of pH = 2.0. The results indicate that no change in RhB dye solution occurs during the temperature change. The RhB degradation performances of the elbaite-alone, H_2O_2-alone and elbaite/H_2O_2 systems were compared. Figure 2b indicates that 16.9% RhB is removed in the elbaite-alone system after 10 min of heating. As a consequence, it can be concluded that elbaite alone also affected the RhB dye solution. When the temperature increased, a polarized electric field was generated on the surface of the elbaite. The dye molecules in the solution are adsorbed by tourmaline elbaite, and this reduces the concentration of the dye solution. Figure 2c shows the N_2 adsorption–desorption isotherm of elbaite powder. According to the adsorption isotherm, the calculated values of specific surface area, pore volume, and pore width are 2.48 m^2/g, 2.2×10^{-2} cm^3/g, and 3.847 nm, respectively. The N_2 adsorption–desorption isotherms indicate that elbaite has a good adsorption capacity compared to other adsorbents [38]. Moreover, there is an obvious red adsorbate on the surface of elbaite after the reaction shown in the inset of Figure 2c. It is reported that the major surface functional group ·OH in tourmaline is responsible for the adsorption of the dye molecule [38]. The increase in the concentration of the RhB solution at 20 and 30 min of heating may come from the slightly evaporated water as the reaction is carried out. Compared with the elbaite alone system, the degradation rate of RhB is 24.8% in the H_2O_2 only system, indicating that RhB can directly react with H_2O_2 without the catalyst. However, the degradation rate of RhB in the elbaite/H_2O_2 system is much higher than in the other two systems. The RhB degradation percentage is 100% at 30 min of heating, with a clear and transparent solution. To investigate the best conditions of the reaction, the impact of different elbaite and H_2O_2 doses on the reaction was investigated.
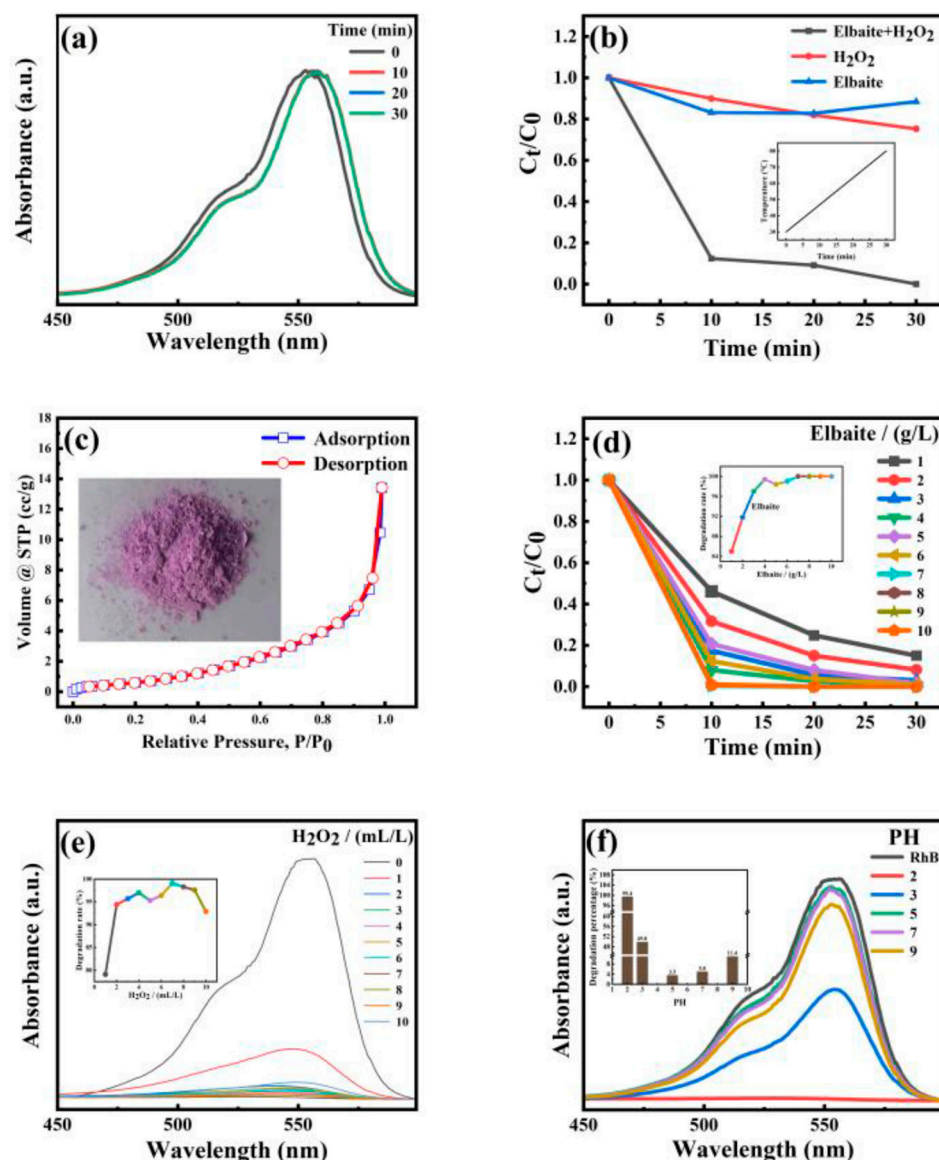
Figure 2. (**a**) Pyrocatalytic UV absorption spectrum of RhB without catalyst. (**b**) RhB removal rates in three different systems. (**c**) N2 adsorption–desorption isotherm of elbaite powder and the picture of elbaite powder after adsorption reaction. (**d**) Effect of elbaite dose on RhB degradation in the elbaite/H_2O_2 system, and the degradation rate of different elbaite doses. (**e**) Effect of H_2O_2 dose on RhB degradation in the elbaite/H_2O_2 system, and the degradation rate of different H_2O_2 doses. (**f**) Effect of initial pH on the degradation of RhB in the elbaite/H_2O_2 system, and the degradation rate at different pH. Experimental conditions: RhB = 100 mg/L, elbaite dose = 1.0–10.0 g/L, H_2O_2 dose = 1.0–10.0 mL/L, initial pH = 2.0, initial pH = 2.0, 3.0, 5.0, 7.0, 9.0, T = 30 °C–80 °C, time = 30 min.

As shown in Figure 2d, the dose of H_2O_2 is 7.0 mL/L, and the degradation efficiency of RhB increases significantly when the elbaite dose changes from 1.0 g/L to 4.0 g/L, reaching 99.4% at 4.0 g/L. With a further increase in the dose of elbaite, the degradation efficiency sinks slightly and then increases gradually to 100% at 7.0 g/L. This is due to the excessive addition of elbaite. On the one hand, the collision frequency between the elbaite particles may enhance the contact between positive and negative charges on the surface of the elbaite. On the other hand, the excessive addition of elbaite leads to a decrease in the dose of charge that can produce the active species. That is, excess elbaite does not lead to higher degradation efficiency. However, as the dose of elbaite continues to increase, the amount of charge generated increases, eliminating these effects. Therefore,

the optimum dose of elbaite was found to be 4.0 g/L. Based on the above results, the dose of elbaite was designated at 4.0 g/L for further study.

The effect of H_2O_2 dose was examined in the elbaite/H_2O_2 system (given in Figure 2e). Firstly, the dose of elbaite was designated as 4.0 g/L. Then, with the increase in H_2O_2 dose from 1.0 mL/L to 7.0 mL/L, the degradation rate increased from 79.1% to 99.1%. After that, when the H_2O_2 dose was increased to 10.0 mL/L, the degradation rate decreased slightly, reaching 92.9%. The results also proved that the degradation rate changed significantly with the dose of H_2O_2. Hence, ·OH is the predicted active substance in the solution, and the direction of change can be explained as follows. With the increase in H_2O_2 dose, H_2O_2 will constantly generate ·OH to attack the RhB structure. However, H_2O_2 is also a scavenger of ·OH. Excess H_2O_2 consumes ·OH before these can react with organic pollutants, which can be explained by reaction Equations (1) and (2) [44,45]. As a result, the optimal efficiency for H_2O_2 is 7.0 mL/L. Thus, 7.0 mL/L H_2O_2 was chosen for further study.

$$H_2O_2 + \cdot OH \rightarrow H_2O + \cdot HO_2 \tag{1}$$

$$HO_2 + \cdot OH \rightarrow H_2O + O_2 \tag{2}$$

In order to study the influence of pH on RhB degradation performance, the influence of the initial pH of the RhB solution on the degradation rate under acidic, neutral, and alkaline conditions was studied in the elbaite/H_2O_2 system, and the results are illustrated in Figure 2f. It can be seen that the highest degradation rate is up to 99.4% at pH = 2.0, while the degradation rate is detected to be only 3.5% at pH = 5.0, 5.0% at pH = 7.0, and 11.4% at pH = 9.0. Clearly, the elbaite/H_2O_2 system shows an excellent degradation rate under a strong acid environment (pH = 2.0) compared to the neutral and alkaline conditions. It is speculated that the pyroelectricity of elbaite in acidic conditions is stronger than that in neutral and alkaline conditions, which leads to higher efficiency. Furthermore, it was found that the amount of hydroxyl decreased first and then increased with the increase in pH. The result is shown in Figure S1. Therefore, the elbaite/H_2O_2 system is pH dependent for the degradation of RhB solution and shows high removal efficiency in low pH conditions.

2.3. Detection of Hydroxyl Radicals

To further determine into the mechanism of the elbaite/H_2O_2 system, the surface radical-trapping experiments proceeded. As shown in Figure 3a, the addition of TBA (a quencher of ·OH) [46] significantly inhibited the decomposition of RhB in the elbaite/H_2O_2 system, and the inhibition degree increased with an increase in TBA content. Without the addition of the scavenger, the degradation rate of RhB dye was 89.1% after 10 min of reaction, where the temperature was 46.7 °C. However, the degradation rate was only 13% after the addition of 50 mM TBA. Therefore, it is presumed that ·OH is the dominant radical in the elbaite/H_2O_2 system, because the scavenger TBA can greatly inhibit the degradation of RhB dye.

To monitor the intermediate products of the pyrocatalysis process, we further demonstrated the generation of ·OH radicals in the elbaite/H_2O_2 system by using TA as a probe molecule. TA reacts with the ·OH to produce 2-hydroxyterephthalic acid (·OH capture), a substance with strong fluorescent properties. It emits a unique fluorescence signal under a PL excitation wavelength of 315 nm with a peak around 425 nm [47]. In turn, the intensity of the fluorescence signal of 2-hydroxyterephthalic acid is proportional to the number of ·OH produced in water [48]. As shown in Figure 3b, with the increase in pyrocatalysis time, the fluorescence intensity of 2-Hydroxyterephthalic acid at 425 nm increased, indicating the presence of ·OH.
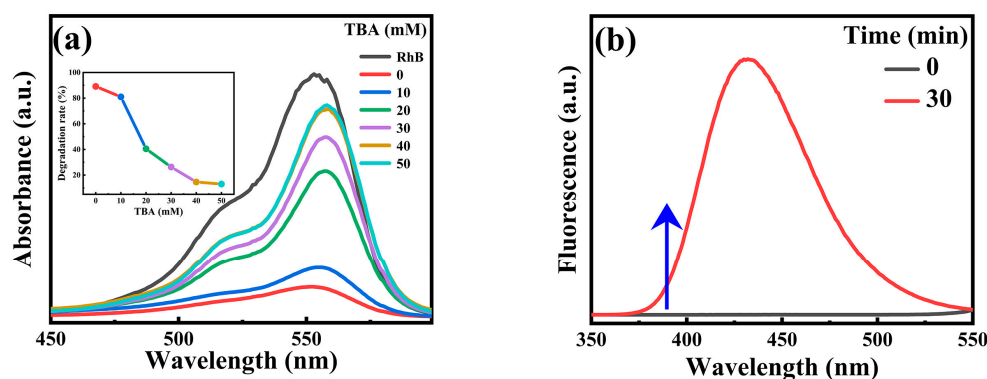
Figure 3. (**a**) The effect of different doses of TBA on the degradation of RhB solution by the elbaite/H_2O_2 system. (**b**) The ·OH capture spectra of suspension containing elbaite and TA were studied at a 315 nm photoluminescence excitation wavelength. Experimental conditions: RhB = 100 mg/L, elbaite dose = 4.0 g/L, H_2O_2 dose = 7.0 mL/L, initial pH = 2.0, T = 30 °C–80 °C, time = 10 min, 30 min.

2.4. Degradation Factors for Contaminant RhB

Reusability and stability are significant and necessary for the practical application of the elbaite/H_2O_2 system. Thus, the recycling utilization of elbaite catalysts was investigated. As shown in Figure 4a, the degradation rate reduced from 100% to 94.5% as the number of cycles increased to three. After three repeated experiments, the degradation rate decreased slightly due to the small loss of elbaite powder during centrifugal filtration. The degradation rate of the third cycle was more than 90% of that of the first cycle, indicating that elbaite has good recycling performance. The FTIR spectra of bare elbaite particles and the elbaite particles after reaction with RhB are shown in Figure 4b. The structure of elbaite in the elbaite/H_2O_2 system is essentially the same before and after the reaction. The bands at 781 cm^{-1} and 1100 cm^{-1} are caused by the stretching vibration of the Si-O-Si bond. The O-Si-O bond and the B-O bond cause stretching vibration at 969 cm^{-1} and 1290 cm^{-1}, respectively. Furthermore, the bonds at 3590 cm^{-1} and 1356 cm^{-1} are the results of the stretching vibration of the O-H bond [49]. It is shown that the reaction process of the elbaite/H_2O_2 system does not cause any change to elbaite, further demonstrating its structural stability. Thus, the excellent recycling performance of elbaite is proved once again.
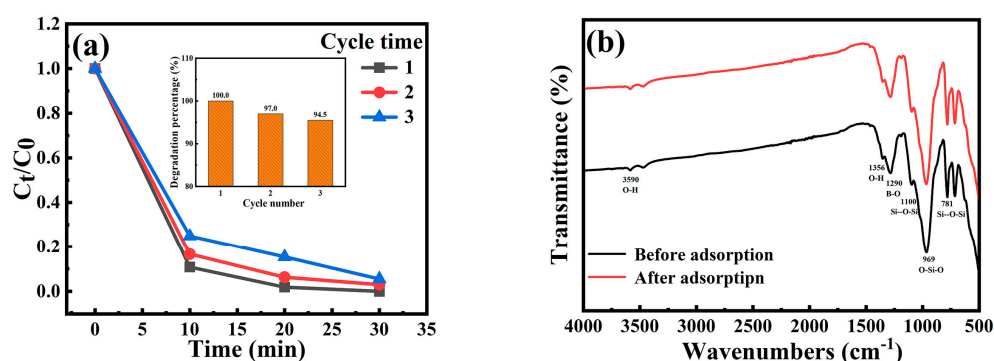

Figure 4. (**a**) Recycling utilization tests with elbaite. (**b**) FTIR spectra of powdered elbaite before reaction and after reaction of the elbaite/H_2O_2 system. Experimental conditions: RhB = 100 mg/L, elbaite dose = 4.0 g/L, H_2O_2 dose = 7.0 mL/L, initial pH = 2.0, T = 30 °C–80 °C, time = 30 min.

2.5. Degradation Factors for Contaminant RhB

The pyroelectricity of elbaite played a major role in the elbaite/H_2O_2 system. The intensity of polarization formed in pyroelectric materials changes as the temperature (T)

changes and, therefore, is defined as the pyroelectric coefficient [50], and the reaction equation is expressed as Equation (3) as follows:

$$P = \frac{\partial P_s}{\partial T} \tag{3}$$

where ∂P_S is the vector of polarization intensity change in the crystal, and ∂T is the small temperature change that occurs uniformly throughout the crystal. The P value represents the strength of the pyro-driven catalytic performance, and the higher the P value, the better the pyro-driven catalytic performance. The polarization intensity (P_s) and pyroelectric coefficient (P) of the selected elbaite at different temperatures were measured by a ferroelectric analyzer. As shown in Figure 5a, the polarization intensity of elbaite changed from 1.30 nC/cm^2 at 30 °C to 7.79 nC/cm^2 at 80 °C. Furthermore, the pyroelectric coefficient of elbaite can reach around 0.20 nC/cm^2/K at 80 °C, according to Figure 5b. The results indicate that the selected elbaite has a relatively high pyroelectric coefficient.
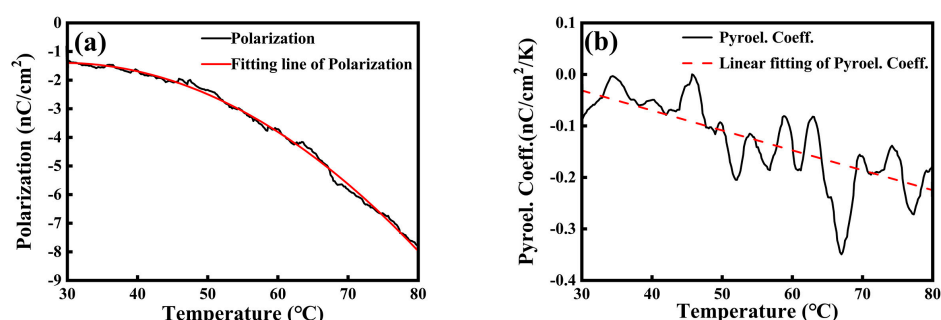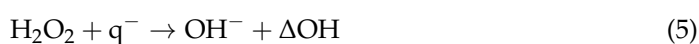

Figure 5. (**a**) Polarization (Ps) and (**b**) pyroelectric coefficient (P) of elbaite.

Figure 6 shows the schematic diagram of pyrocatalysis in the elbaite/H$_2$O$_2$ system. Elbaite contain a high pyroelectric coefficient P of 0.2 nC/cm^2/K. In the case of a thermodynamic equilibrium state ($\Delta T = 0$ °C), the surface of elbaite does not have a polarized charge. When the elbaite particles are heated, the temperature of elbaite particles changes, the total electric dipole moment vector sum decreases, and the polarization density decreases, causing a large amount of polarized charge to accumulate on the surface of elbaite particles, which can be expressed as Equation (4). At the same time, the negative charges react with H$_2$O$_2$ to produce ·OH- and ·OH, as shown in Equation (5). Not only that, but the positive charge (h$^+$) accumulated on the positive charge side of elbaite also reacts with ·OH$^-$ to produce ·OH, as shown in Equation (6). Furthermore, ·OH in the solution causes the dye to decompose through redox reaction so as to achieve the purpose of degradation, as shown in Equation (7) [51,52]. As a result, the pyro-electro-chemical coupling of the elbaite/H$_2$O$_2$ system contributes to the decomposition of RhB.
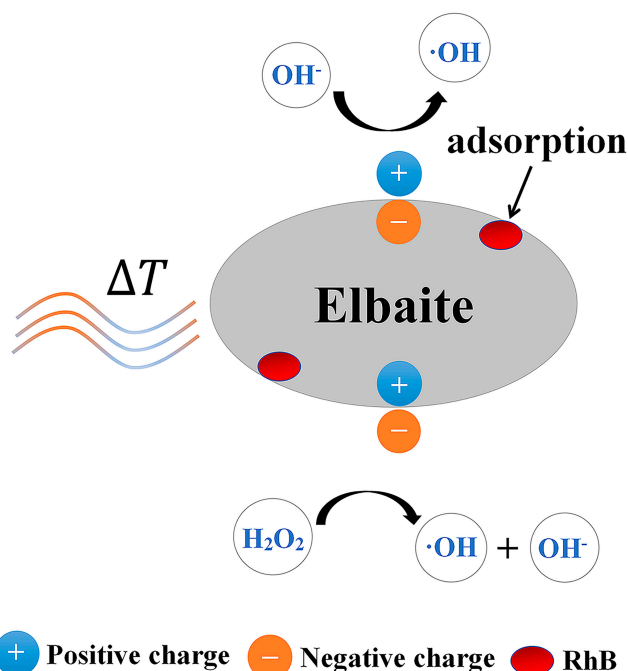
$$\text{Elbaite} \xrightarrow{\Delta T} \text{Elbaite} + h^+ + q^- \tag{4}$$

$$H_2O_2 + q^- \rightarrow OH^- + \Delta OH \tag{5}$$

$$h^+ + OH^- \rightarrow \Delta OH \tag{6}$$

$$OH + Dye \rightarrow Dye\ decomposition \tag{7}$$

Figure 6. Devised mechanism for RhB degradation in the elbaite/H_2O_2 system.

3. Materials and Methods

RhB, TA, and tert-butyl alcohol (TBA) were purchased from Aladdin. Deionized water was used for the preparation of RhB solution. The sodium hydroxide (NaOH) and sulfuric acid (H_2SO_4) that were used in the experiment were purchased from Sinopharm Chemical Reagent Co. H_2O_2 (30%, v/v) was obtained from Nanjing Chemical Reagent Co., Ltd. Elbaite was purchased from Brazil with high purity, and it was ground into micron-sized particles using an intelligent high-throughput tissue grinder. Then, it was washed five times with deionized water, dried at about 80 °C, and stored in a dry container before use. The reagents used in this study are all analytical grade reagents and can be used directly without further purification.

The phases of elbaite were characterized by PANalytical X'pert PRO powder X-ray diffractometer (Cu Kα radiation, λ = 1.5406 Å) with 2θ ranging from 10° to 80° at step width of 0.01°. The morphology of the elbaite powder sample was characterized by using a scanning electron microscope (SEM, The Netherlands). The chemical composition of the elbaite samples was analyzed by energy-dispersive X-ray spectroscopy (EDS, Japan), iCAP Q inductively coupled plasma mass spectrometry (ICP-MS, USA), and EDX-7000 X-ray fluorescence spectrometry (XRF, Japan). The N_2 adsorption isotherm was measured at 77.3 K to determine the specific surface area (S_{BET}) via the Brunauer–Emmett–Teller (BET, autosorb iQ, USA) method, while the total pore volumes (Vtotal) and pore width were directly obtained from the isotherm at P/P_0 = 0.99. The pyroelectricity of the sample was measured using a Ferro-electric Analyzer (TF-3000E, aix-ACCT, Germany) at different temperature ranges, where the elbaite sample was cut into small slices (perpendicular to c-axis) and polished. Furthermore, the size of each slice was approximately 6 mm × 6 mm × 1.0 mm. The upper and lower surfaces of each piece were coated with silver glue. A Fourier transform infrared spectroscopy (FTIR, spectrometer Nicolet Avatar 370DTGS, Thermo, USA) covering a wave number between 500 cm^{-1} and 4000 cm^{-1} was used to identify the functional groups on the bare elbaite particles and the elbaite particles after reaction with RhB.

The pyrocatalytic activities of the elbaite/H_2O_2 system were diagnosed through the degradation situation of RhB aqueous solution (100 mg/L). The degradation experiments were implemented in a thermostatic water bath. In the degradation experiments, elbaite was immersed in 100 mL of RhB aqueous solution and stirred for ~1 h to establish

an adsorption–desorption equilibrium between the elbaite and the RhB solution. Then, the H_2O_2 aqueous solution was added into the mixture solution, where the pH was adjusted to 2 by using H_2SO_4 and NaOH. The solution was heated from 30 °C to 80 °C at a constant rate in a water bath within 30 min to make full use of pyroelectric properties. Then, 5 mL of RhB aqueous solution was taken out and centrifuged at 11,000 rpm for 2 min in a TG20-WS table top high-speed centrifuge (China) to remove impurities. Accordingly, the concentration of RhB aqueous solution was measured using a UV–Vis spectrophotometer (T6, Beijing Puxi General Instrument Co. Ltd.). For comparison, adsorption capacity of elbaite was determined by an adsorption experiment. Elbaite was added to RhB aqueous solution and stirred for ~1 h without H_2O_2, and the experiment conditions were the same as for the elbaite/H_2O_2 system. In addition, H_2O_2 was added to RhB aqueous solution without elbaite to determine its effect on the solution, and the experiment conditions were the same as those used for the elbaite/H_2O_2 system. RhB concentration was detected during the reaction, and the change in RhB concentration can reflect the adsorption capacity of elbaite. Here, the degradation rate (DR) was calculated using the following equation:

$$DR\ (\%) = 1 - C_t/C_0 \times 100\% \tag{8}$$

where C_0 and C_t denote the premier and residual RhB concentration at t min, respectively, and DR is the final degradation rate. Subsequently, the influence of various factors on RhB degradation efficiency was investigated. Firstly, the optimum dose of elbaite (1.0–10.0 g/L) was researched during the reaction progress. Secondly, we explored the optimum dose of H_2O_2 (1.0–10.0 mL/L). Afterwards, the initial pH of RhB solution was designed to 2.0, 3.0, 5.0, 7.0, and 9.0 with 0.5 mol/L H_2SO_4 or NaOH aqueous solution to reveal the pH dependence of the elbaite/H_2O_2 system. Finally, the recyclability of the elbaite/H_2O_2 system was tested. During the recycling experiment, the elbaite particles were collected by centrifugation and washed by deionized water and ethanol five times. Afterwards, the collected elbaite was dried to a constant weight in an oven at 80 °C. The experiment was repeated for the second and third cycles.

In order to verify the active substances produced in the pyrocatalysis process, the TBA trapping experiment was performed [46]. During the pyrocatalysis process, TBA was added into the optimal elbaite/H_2O_2 system with the content ranging from 10–50 mM. RhB aqueous solution concentration changes with time, thus confirming the role of ·OH in the pyrocatalysis process. In order to further determine the presence of ·OH, the photoluminescence (PL) technique of terephthalic acid (TA) as probe molecule was used to achieve more accurate detection of ·OH radical induced pyroelectrically [48]. TA reacts with ·OH to produce 2-hydroxyl terephthalic acid, which presents a highly fluorescent state with a peak center at 425 nm, and its PL intensity is positively correlated with the amount of ·OH produced in water [47,53]. Definitively, 2 mM NaOH and 0.5 mM TA were mixed into the 100mL aqueous solution, and then the solution was transferred to the RhB aqueous solution. Thereafter, elbaite was added to RhB aqueous solution and stirred for 1 h to establish the adsorption–desorption equilibrium between elbaite and solution. The result is shown in Figure S2. Finally, 0.7 mL H_2O_2 was added, and the solution was transferred to the same experimental procedure. At the excitation wavelength of 315 nm, the PL intensity of the solution was measured at different reaction times.

4. Conclusions

An elbaite/H_2O_2 pyro-electro-chemical coupling catalytic system was developed and successfully applied to the degradation of RhB aqueous solution. Extensive degradation experiments showed that the optimized degradation efficiency of RhB reached 100.0% at 4.0 g/L elbaite, 7.0 mL/L H_2O_2, and pH = 2.0 in the elbaite/H_2O_2 system. Recycling utilization showed that the third removal rate was 94.5%, which demonstrates the economic usefulness of the silicate mineral elbaite. Furthermore, it is shown that ·OH was the main active specie involved in catalytic degradation in the elbaite/H_2O_2 pyro-electro-chemical coupling catalytic system. Elbaite plays the role of a dye sorbent and a pyroelectric catalyst

to activate H_2O_2 in order to generate the primary ·OH for subsequent advanced redox reactions. Therefore, the effective application of the elbaite/H_2O_2 pyroelectric catalytic system has a high potential for the purification of dye wastewater.

Supplementary Materials: The following are available online at https://www.mdpi.com/article/10.3390/catal11111370/s1, Figure S1. The ·OH capture (TA) spectra of suspension at different pH. Figure S2. Pyrocatalytic UV absorption spectrum of RhB after adsorption-desorption.

Author Contributions: D.M. and C.Z. conceived and designed the experiments; F.C. and J.G. performed the pyro-electro-chemical catalytic experiments and measured the strong oxidation actives; F.C. and J.G. described the mechanism of the elbaite/H_2O_2 system; R.S. and Y.W. conducted the XRD, SEM, ICP-MS, XRF, and BET experiments and performed recycling; F.C. wrote the original draft. All authors have read and agreed to the published version of the manuscript.

Data Availability Statement: The data presented in this study are available on request from the corresponding authors.

Conflicts of Interest: The authors declare no conflict of interest.

References

1. Ahmad, A.; Mohd-Setapar, S.H.; Chuong, C.S.; Khatoon, A.; Wani, W.A.; Kumar, R.; Rafatullah, M. Recent advances in new generation dye removal technologies: Novel search for approaches to reprocess wastewater. *RSC Adv.* **2015**, *5*, 30801–30818. [CrossRef]
2. Lin, H.; Wu, Z.; Jia, Y.; Li, W.; Zheng, R.K.; Luo, H. Piezoelectrically induced mechano-catalytic effect for degradation of dye wastewater through vibrating Pb ($Zr_{0.52}Ti_{0.48}$) O_3 fibers. *Appl. Phys. Lett.* **2014**, *104*, 162907. [CrossRef]
3. Krawczyk, K.; Wacławek, S.; Kudlek, E.; Silvestri, D.; Kukulski, T.; Grübel, K.; Černík, M.; Padil, V.V.T. UV-catalyzed persulfate oxidation of an anthraquinone based dye. *Catalysts* **2020**, *10*, 456. [CrossRef]
4. Forgacs, E.; Cserhati, T.; Oros, G. Removal of synthetic dyes from wastewaters: A review. *Environ. Int.* **2004**, *30*, 953–971. [CrossRef]
5. Xu, Y.; Li, X.; Cheng, X.; Sun, D.; Wang, X. Degradation of cationic red GTL by catalytic wet air oxidation over Mo–Zn–Al–O catalyst under room temperature and atmospheric pressure. *Environ. Sci. Technol.* **2012**, *46*, 2856–2863. [CrossRef] [PubMed]
6. Mat Yasin, N.M.F.; Hossain, M.S.; HPS., A.K.; Zulkifli, M.; Al-Gheethi, A.; Asis, A.J.; Yahaya, A.N. Treatment of palm oil refinery effluent using tannin as a polymeric coagulant: Isotherm, kinetics, and thermodynamics analyses. *Polymers* **2020**, *12*, 2353. [CrossRef] [PubMed]
7. Anjaneyulu, Y.; Chary, N.S.; Raj, D.S.S. Decolourization of industrial efflfluents–Available methods and emerging technologies—A review. *Rev. Environ. Sci. Bio/Technol.* **2005**, *4*, 245–273. [CrossRef]
8. Sutherland, J.; Adams, C.; Kekobad, J. Treatment of MTBE by air stripping, carbon adsorption, and advanced oxidation: Technical and economic comparison for five groundwaters. *Water Res.* **2004**, *38*, 193–205. [CrossRef]
9. Chiang, K.Y.; Wang, K.S.; Lin, F.L.; Chu, W.T. Chloride effects on the speciation and partitioning of heavy metal during the municipal solid waste incineration process. *Sci. Total Environ.* **1997**, *203*, 129–140. [CrossRef]
10. Cimini, S.; Prisciandaro, M.; Barba, D. Simulation of a waste incineration process with flue-gas cleaning and heat recovery sections using Aspen Plus. *Waste Manag.* **2005**, *25*, 171–175. [CrossRef]
11. Zagklis, D.P.; Vavouraki, A.I.; Kornaros, M.E.; Paraskeva, C.A. Purification of olive mill wastewater phenols through membrane filtration and resin adsorption/desorption. *J. Hazard. Mater.* **2015**, *285*, 69–76. [CrossRef]
12. Boucher, F.R.; Lee, G.F. Adsorption of lindane and dieldrin pesticides on unconsolidated aquifer sands. *Environ. Sci. Technol.* **1972**, *6*, 538–543. [CrossRef]
13. Martinez-Huitle, C.A.; Ferro, S. Electrochemical oxidation of organic pollutants for the wastewater treatment: Direct and indirect processes. *Chem. Soc. Rev.* **2006**, *35*, 1324–1340. [CrossRef]
14. Lin, S.H.; Chuang, T.S. Combined treatment of phenolic wastewater by wet air oxidation and activated sludge. *Toxicol. Environ. Chem.* **1994**, *44*, 243–258. [CrossRef]
15. Scott, J.P.; Ollis, D.F. Integration of chemical and biological oxidation processes for water treatment: Review and recommendations. *Environ. Prog.* **1995**, *14*, 88–103. [CrossRef]
16. Wang, Y.-T. Effect of chemical oxidation on anaerobic biodegradation of model phenolic compounds. *Water Environ. Res.* **1992**, *64*, 268–273. [CrossRef]
17. Munter, R. Advanced oxidation processes–current status and prospects. *Proc. Est. Acad. Sci. Chem.* **2001**, *50*, 59–80. [CrossRef]
18. Augugliaro, V.; Bellardita, M.; Loddo, V.; Palmisano, G.; Palmisano, L.; Yurdakal, S. Overview on oxidation mechanisms of organic compounds by TiO_2 in heterogeneous photocatalysis. *J. Photoch. Photobio. C Photochem. Rev.* **2012**, *13*, 224–245. [CrossRef]

19. Yurdakal, S.; Palmisano, G.; Loddo, V.; Augugliaro, V.; Palmisano, L. Nanostructured rutile TiO$_2$ for selective photocatalytic oxidation of aromatic alcohols to aldehydes in water. *J. Am. Chem. Soc.* **2008**, *130*, 1568–1569. [CrossRef]

20. Augugliaro, V.; Prevot, A.B.; Vázquez, J.C.; Garcıa-López, E.; Irico, A.; Loddo, V.; Malato Rodrıguez, S.; Marcı, G.; Palmisano, L.; Pramauro, E. Photocatalytic oxidation of acetonitrile in aqueous suspension of titanium dioxide irradiated by sunlight. *Adv. Environ. Res.* **2004**, *8*, 329–335. [CrossRef]

21. Marin, M.L.; Santos-Juanes, L.; Arques, A.; Amat, A.M.; Miranda, M.A. Organic photocatalysts for the oxidation of pollutants and model compounds. *Chem. Rev.* **2012**, *112*, 1710–1750. [CrossRef]

22. Martinez-Haya, R.; Luna, M.M.; Hijarro, A.; Martinez-Valero, E.; Miranda, M.A.; Marin, M.L. Photocatalytic degradation of phenolic pollutants using N-methylquinolinium and 9-mesityl-10-methylacridinium salts. *Catal. Today* **2019**, *328*, 243–251. [CrossRef]

23. Martinez-Haya, R.; Gomis, J.; Arques, A.; Marin, M.L.; Amat, A.M.; Miranda, M.A. Time-resolved kinetic assessment of the role of singlet and triplet excited states in the photocatalytic treatment of pollutants at different concentrations. *Appl. Catal. B-Environ.* **2017**, *203*, 381–388. [CrossRef]

24. Zhu, Y.; Zhu, R.; Xi, Y.; Zhu, J.; Zhu, G.; He, H. Strategies for enhancing the heterogeneous Fenton catalytic reactivity: A review. *Appl. Catal. B-Environ.* **2019**, *255*, 117739. [CrossRef]

25. Wang, A.; Wang, H.; Deng, H.; Wang, S.; Shi, W.; Yi, Z.; Yan, K. Controllable synthesis of mesoporous manganese oxide microsphere efficient for photo-Fenton-like removal of fluoroquinolone antibiotics. *Appl. Catal. B-Environ.* **2019**, *248*, 298–308. [CrossRef]

26. Wang, J.; Wang, S. Activation of persulfate (PS) and peroxymonosulfate (PMS) and application for the degradation of emerging contaminants. *Chem. Eng. J.* **2018**, *334*, 1502–1517. [CrossRef]

27. Jiang, L.; Zhang, Y.; Zhou, M.; Liang, L.; Li, K. Oxidation of Rhodamine B by persulfate activated with porous carbon aerogel through a non-radical mechanism. *J. Hazard. Mater.* **2018**, *358*, 53–61. [CrossRef] [PubMed]

28. Ribeiro, A.R.; Nunes, O.C.; Pereira, M.F.; Silva, A.M. An overview on the advanced oxidation processes applied for the treatment of water pollutants defined in the recently launched Directive 2013/39/EU. *Environ. Int.* **2015**, *75*, 33–51. [CrossRef]

29. Mezyk, S.P.; Neubauer, T.J.; Cooper, W.J.; Peller, J.R. Free-radical-induced oxidative and reductive degradation of sulfa drugs in water: Absolute kinetics and efficiencies of hydroxyl radical and hydrated electron reactions. *J. Phys. Chem. A* **2007**, *111*, 9019–9024. [CrossRef] [PubMed]

30. Sebald, G.; Guyomar, D.; Agbossou, A. On thermoelectric and pyroelectric energy harvesting. *Smart Mater. Struct.* **2009**, *18*, 125006. [CrossRef]

31. Lang, S.B.; Muensit, S. Review of some lesser-known applications of piezoelectric and pyroelectric polymers. *Appl. Phys. A* **2006**, *85*, 125–134. [CrossRef]

32. Xu, X.; Chen, S.; Wu, Z.; Jia, Y.; Xiao, L.; Liu, Y. Strong pyro-electro-chemical coupling of Ba$_{0.7}$Sr$_{0.3}$TiO$_3$@Ag pyroelectric nanoparticles for room-temperature pyrocatalysis. *Nano Energ.* **2018**, *50*, 581–588. [CrossRef]

33. You, H.; Wu, Z.; Wang, L.; Jia, Y.; Li, S.; Zou, J. Highly efficient pyrocatalysis of pyroelectric NaNbO$_3$ shape-controllable nanoparticles for room-temperature dye decomposition. *Chemosphere* **2018**, *199*, 531–537. [CrossRef] [PubMed]

34. Xia, Y.; Jia, Y.; Qian, W.; Xu, X.; Wu, Z.; Han, Z.; Hong, Y.; You, H.; Ismail, M.; Bai, G. Pyroelectrically induced pyro-electro-chemical catalytic activity of BaTiO$_3$ nanofibers under room-temperature cold–hot cycle excitations. *Metals* **2017**, *7*, 122. [CrossRef]

35. Qian, W.; Wu, Z.; Jia, Y.; Hong, Y.; Xu, X.; You, H.; Zheng, Y.; Xia, Y. Thermo-electro-chemical coupling for room temperature thermocatalysis in pyroelectric ZnO nanorods. *Electrochem. Commun.* **2017**, *81*, 124–127. [CrossRef]

36. Ma, J.; Chen, L.; Wu, Z.; Chen, J.; Jia, Y.; Hu, Y. Pyroelectric Pb (Zr$_{0.52}$Ti$_{0.48}$) O$_3$ polarized ceramic with strong pyro-driven catalysis for dye wastewater decomposition. *Ceram. Int.* **2019**, *45*, 11934–11938. [CrossRef]

37. Zhou, G.; Liu, H.; Chen, K.; Gai, X.; Zhao, C.; Liao, L.; Shan, Y. The origin of pyroelectricity in tourmaline at varying temperature. *J. Alloys Compd.* **2018**, *744*, 328–336. [CrossRef]

38. Liu, N.; Wang, H.; Weng, C.H.; Hwang, C.C. Adsorption characteristics of Direct Red 23 azo dye onto powdered tourmaline. *Arab. J. Chem.* **2018**, *11*, 1281–1291. [CrossRef]

39. Shi, J.; Yin, D.; Xu, Z.; Song, D.; Cao, F. Fosfomycin removal and phosphorus recovery in a schorl/H$_2$O$_2$ system. *RSC Adv.* **2016**, *6*, 68185–68192. [CrossRef]

40. Zhang, Y.; Shi, J.; Xu, Z.; Chen, Y.; Song, D. Degradation of tetracycline in a schorl/H$_2$O$_2$ system: Proposed mechanism and intermediates. *Chemosphere* **2018**, *202*, 661–668. [CrossRef] [PubMed]

41. Tokumura, M.; Znad, H.T.; Kawase, Y. Modeling of an external light irradiation slurry photoreactor: UV light or sunlight-photoassisted Fenton discoloration of azo-dye Orange II with natural mineral tourmaline powder. *Chem. Eng. Sci.* **2006**, *61*, 6361–6371. [CrossRef]

42. Li, J.; Wang, C.; Wang, D.; Zhou, Z.; Sun, H.; Zhai, S. A novel technology for remediation of PBDEs contaminated soils using tourmaline-catalyzed Fenton-like oxidation combined with P. chrysosporium. *Chem. Eng. J.* **2016**, *296*, 319–328. [CrossRef]

43. Zhang, X.H.; Wu, R.H. Mechanism and experimental Research on improvement in conductive performances of ZnO coated tourmaline powder. *Adv. Mat. Res.* **2013**, *750*, 2108–2112. [CrossRef]

44. Zhang, H.; Wu, J.; Wang, Z.; Zhang, D. Electrochemical oxidation of crystal violet in the presence of hydrogen peroxide. *J. Chem. Technol. Biotechnol.* **2010**, *85*, 1436–1444. [CrossRef]

45. Li, Y.; Lu, Y.; Zhu, X. Photo-Fenton discoloration of the azo dye X-3B over pillared bentonites containing iron. *J. Hazard. Mater.* **2006**, *132*, 196–201. [CrossRef]

46. Xu, T.; Cai, Y.; O'Shea, K.E. Adsorption and photocatalyzed oxidation of methylated arsenic species in TiO_2 suspensions. *Environ. Sci. Technol.* **2007**, *41*, 5471–5477. [CrossRef]

47. Yu, J.; Wang, W.; Cheng, B.; Su, B.L. Enhancement of photocatalytic activity of mesporous TiO_2 powders by hydrothermal surface fluorination treatment. *J. Mater. Chem. C* **2009**, *113*, 6743–6750. [CrossRef]

48. Xu, X.; Wu, Z.; Xiao, L.; Jia, Y.; Ma, J.; Wang, F.; Huang, H. Strong piezo-electro-chemical effect of piezoelectric $BaTiO_3$ nanofibers for vibration-catalysis. *J. Alloys Compd.* **2018**, *762*, 915–921. [CrossRef]

49. Li, G.; Chen, D.; Zhao, W.; Zhang, X. Efficient adsorption behavior of phosphate on La-modified tourmaline. *J. Environ. Chem. Eng.* **2015**, *3*, 515–522. [CrossRef]

50. Damjanovic, D. Ferroelectric, dielectric and piezoelectric properties of ferroelectric thin films and ceramics. *Rep. Prog. Phys.* **1998**, *61*, 1267. [CrossRef]

51. Zhan, H.; Tian, H. Photocatalytic degradation of acid azo dyes in aqueous TiO_2 suspension I, The effect of substituents. *Dye. Pigment.* **1998**, *37*, 231–239. [CrossRef]

52. Houas, A.; Lachheb, H.; Ksibi, M.; Elaloui, E.; Guillard, C.; Herrmann, J.M. Photocatalytic degradation pathway of methylene blue in water. *Appl. Catal. B* **2001**, *31*, 145–157. [CrossRef]

53. Xiao, Q.; Si, Z.; Zhang, J.; Xiao, C.; Tan, X. Photoinduced hydroxyl radical and photocatalytic activity of samarium-doped TiO_2 nanocrystalline. *J. Hazard. Mater.* **2008**, *150*, 62–67. [CrossRef] [PubMed]